

# Simvastatin-loaded 3D aerogel scaffolds promote bone regeneration

Lai Linfeng<sup>a,b,c</sup>, Zhou Xiaowei<sup>a,b,c,d</sup>, Chen Xueqin<sup>a,b,c</sup> and Zhu Xianfeng<sup>a,b,c,\*</sup>

<sup>a</sup>Dingling Clinical College, Wenzhou Medical University, Wenzhou, China

<sup>b</sup>Wenzhou Central Hospital, Wenzhou, China

<sup>c</sup>The Second Affiliated Hospital of Shanghai University, Wenzhou, China

<sup>d</sup>Wenzhou Renmin Hospital, Wenzhou, China

Received 21 April 2023

Accepted 13 November 2023

## Abstract.

**BACKGROUND:** It is imperative to design a suitable material for bone regeneration that emulates the microstructure and compositional framework of natural bone while mitigating the shortcomings of current repair materials.

**OBJECTIVE:** The aim of the study is to synthesize a 3D aerogel scaffold composed of PLCL/gelatin electro-spun nanofiber loaded with Simvastatin and investigate its biocompatibility as well as its performance in cell proliferation and ossification differentiation.

**METHODS:** PLCL/gelatin nanofibers were fabricated in coaxial electrospinning with simvastatin added. Fibers were fragmented, pipetted into molds, frozen, and dried. The morphology of fibers and contact angles in 4 groups of PLCL, PLCL@S, 3D-PLCL, and 3D-PLCL@S was observed and compared. MC3T3-E1 cells were planted at the four materials to observe cell growth status, and ALP and ARS tests were conducted to compare the ossification of cells.

**RESULTS:** TEM scanning showed the coaxial fiber of the inner PLCL and outer gelatin. The mean diameter of the PLCL/gelatin fibers is  $561 \pm 95$  nm and  $631 \pm 103$  nm after the drug loading. SEM showed the fibers in the 3D-PLCL@S group were more curled and loose with more space interlaced. The contact angle in this group was  $27.1^\circ$ , the smallest one. Drug release test demonstrated that simvastatin concentration in the 3D-PLCL@S could remain at a relatively high level compared to the control group. The cell proliferation test showed that MC3T3-E1 cells could embed into the scaffold deeply and exhibit higher viability in the 3D-PLCL@S group than other groups. The ossification tests of ALP and ARS also inferred that the 3D-PLCL@S scaffold could offer a better osteogenic differentiation matrix.

**CONCLUSION:** The PLCL/gelatin aerogel scaffold, when loaded with Simvastatin, demonstrates a more pronounced potential in enhancing osteoblast proliferation and osteogenic differentiation. We hypothesize that this scaffold could serve as a promising material for addressing bone defects.

Keywords: 3D scaffold, aerogel, bone regeneration, simvastatin

## 1. Background

The number of patients with bone defects due to a variety of reasons, such as injuries, infection, and tumors, are increasing recently, which has created a need for bone regenerative processes [1,2].

---

\* Corresponding author: Zhu Xianfeng. E-mail: [Xianfeng\\_Zhu@outlook.com](mailto:Xianfeng_Zhu@outlook.com).

Autologous bone could repair some small defects, but the large bone defects ( $>1\text{--}3$  cm, depending on the anatomical site) may not repair depending on the reserving bone, which could cause bone-derived surrounding tissues to be injured, prolong the treatment time and may sometimes require secondary operation, causing the patients pain [3–5]. This reminds us that there is a huge insufficiency of bone repair tissue, including the Allograft, artificial bone. The allograft bone is still controversial in the study of transplantation and immunity, transplantation and infection behind the virtues of similarity to the autograft at intensity and structure [3,6]. Artificial bone tissues have become a hot research topic and the ideal artificial bone material has the advantages of good biocompatibility, bone conductivity, bone inducibility, degradation, etc. The artificial bone material commonly used in the clinic includes inorganic bone, organic bone, and composite bone material [7,8].

Bone trabecular bio-mimics can provide structural support in bone defects. Its elasticity is similar to bone, and its average porosity can reach 80% [9]. Fully interconnected pores provide pathways for cell growth, and it has the advantages of a porous coating surface, good biocompatibility, and corrosion resistance [10–12]. The biomimetic materials of bone trabeculae reported recently, such as titanium alloy and other metal materials, hydroxyapatite and other ceramic materials, collagen, and other natural biological materials, all have obvious drawbacks [13,14]. Therefore, it is necessary to find a synthetic organic polymer material to simulate the microstructure and composition structure of natural bone. Previous studies have found that organic polymer materials such as hydrogels can be used as scaffolds to support the growth of cells and tissues, and degrade after the tissue grows firmly [15,16].

Compared with hydrogels, aerogels have become a better choice for bone regeneration due to their high porosities and low densities and are easy for cell adherence and proliferation [17]. Three-dimensional (3D) aerogel scaffolds especially are suitable for bone regeneration materials for their better biocompatibility and biodegradability [18]. A recent study has reported that a hybrid nanofiber was composed of electro-spun poly(lactic-co-glycolic) acid-collagen-gelatin (PLGA-PCG) nanofibers and strontium-copper co-doped bio-glass (Sr-Cu-BG) nanofibers in cranial bone regeneration and loaded with a biomolecule of E7-BMP-2. After being implanted into a defective region of rats, a series of research showed 65% closure of the defect bone after 8 weeks, which reminds us that 3D aerogel could be a potential tissue engineering scaffold for bone repair [19]. Therefore, we decided to investigate a 3D polycaprolactone (PLCL) aerogel loaded with relevant drugs could be another choice for the repair of the bone defect.

Besides, simvastatin has been reported to promote osteoblast activity and inhibit osteoclast activity. Simvastatin induces osteoblast differentiation by promoting bone morphogenetic protein 2 (BMP-2) expression by antagonizing TNF- $\alpha$  to Ras/Rho/Mitogen-activated protein kinase pathways and increasing BMP-smad signaling [20,21]. Based on this, in the study, a 3D PLCL aerogel of simvastatin-controlled releasing was constructed to explore whether it is a better composite nano-repair scaffold to promote bone repair.

## 2. Methods

### 2.1. Fabrication of PLCL/gelatin nanofibers and 3D aerogel scaffold

To electrospin the PLCL/gelatin nanofibers, PLCL (Mw80,000, 8 wt%) and gelatin (from porcine skin powder, Type A, Sigma Aldrich, 4 wt%) were dissolved separately in TFE, stirred for 5 to 6 h to get a homogenous solution respectively and simvastatin was added into the PCL solution (simvastatin: PLCL 1:3). Next, coaxial electrospinning was used to form the inner layer of PLCL, whereas conjugated

electrospinning was used to form the outer layer of the nanofiber with a volume flow rate of 0.5 ml/h for the core solution and 2.5 ml/h for shell solution via two syringe pumps. The outer and inner tubes had a mean diameter of 0.56 and 0.34  $\mu\text{m}$ , respectively. An electrostatic field force was created by applying a current of about 20 kV voltages to introduce the formation of nanofibers. The nanofiber membranes were collected at the vacuum drier to volatile solvent for 5 days.

To obtain the 3D aerogel, the fibers were fragmented into broken segments by the probe sonicator in the ice-cold condition. Next, the fiber suspensions were pipetted into molds and frozen rapidly by cryopreserved ethanol in a  $-80^\circ\text{C}$  freezer, which was transferred into the lyophilizer to be dried at  $-60^\circ\text{C}$  for 72 h. The samples were put into the absolute ethanol container in the warm water bath for 10 min and after 3 times solvent exchange with deionized water, the samples were put into the vacuum to remove the bubbles in the aerogel. Finally, the samples were shaped according to the experimental needs [19,22].

Characterization of the coaxial electrospun fibers and 3D nanofiber aerogels. The morphology of the electrospun fibers was checked with transmission electron microscopy (TEM, JEOL 1200EX) and the morphology of the 3D nanofiber aerogels were characterized by scanning electron microscopy (FE-SEM; Hitachi S4700). The contact angle of four different scaffold membranes was carried out by static water contact angle measurement (Automatic Contact Angle Meter Model SL200B, China) [23].

## 2.2. Simvastatin release test

To compare simvastatin load and release between 3D-PLCL@S and PLCL@S, we punched the two nanofiber membranes into uniform disks with a diameter of 6 mm and put the single disk into the 200  $\mu\text{L}$  PBS respectively at the 48-well plates, which were incubated in the cell incubator at  $37^\circ\text{C}$ . From the incubating day on, the simvastatin concentration was measured by ultraviolet-visible spectrophotometry every 2 days and then the solution was refreshed with new PBS of 200  $\mu\text{L}$  after the observation until the next observation.

## 2.3. Cell culture

Mouse pre-osteoblast MC3T3-E1 cells were purchased from ATCC, which were seeded onto the discs and cultured in  $\alpha$ -MEM(Gibco) with 10% fetal bovine serum (FBS, Gibco) and 1% penicillin/streptomycin (Gibco) at  $37^\circ\text{C}$  and 5%  $\text{CO}_2$ . The cells were trypsinized, resuspended, and seeded individually onto culture dishes at the density of  $1 \times 10^4$  cells/mL for further proliferation and the next experiment.

## 2.4. Cell proliferation test

To study the influence of simvastatin-loaded 3D aerogel nanofibers on cell proliferation, five different groups of materials (PLCL, 3D-PLCL, PLCL@S, 3D-PLCL@S, and Cover Slip) were punched into 6 mm disks and put on the 48-well plates. Cover slip group is the blank control group.  $5 \times 10^4$  MC3T3-E1 cells were planted on the materials at the cell incubator of  $37^\circ\text{C}$  with 5%  $\text{CO}_2$ . At the 3-day points of 1, 4, and 7 after plantation, the cell viability was examined by the CCK8 reagent through a spectrophotometer. The result was analyzed with GraphPad 8.0.

## 2.5. Cell attachment and morphology

Cells were planted at the four different groups of materials as above, including the PLCL/gelatin membrane group (PLCL), PLCL/gelatin membrane with simvastatin loaded (PLCL@S), PLCL/gelatin

3D aerogel membrane (3D-PLCL) and PLCL/gelatin 3D aerogel membrane with simvastatin loaded (3D-PLCL@S). On D4 and D7, samples were washed with PBS 3 times and fixed at the 4% paraformaldehyde for 2 h and treated with 0.5% Triton X-100 for 10 min. Through 30 min treatment of phalloidin and 15 min of DAPI in dark, samples were transferred to the confocal plates and the cells living in the different materials were observed by the confocal microscope. Besides, the cell growth deep in the 3D-PLCL@S was shown through the 3D reconstruction model drawn by the ARIVIS VISION.

### 2.6. ALP and Alizarin Red S Staining

MC3T3-E1 cells were cultured in osteogenic medium until D7 and D14 respectively at 4 different materials, washed 3 times with PBS, and stained as an instrument of ALP staining kit (Sigma-Aldrich). As for Alizarin Red S Staining (ARS), same as the cell differentiation of ALP staining, cells were fixed with 70% ethanol for 2 h, washed with PBS, and stained with ARS kit (Sigma-Aldrich, 40 nM) for 10 min and washed. Then we observed the stain performance through the Leica microscope. ALP stain photographs were analyzed through imageJ. *T* tests were conducted to analyze the significance.

## 3. Results

### 3.1. Characteristic of the PLCL fiber with simvastatin

The basic fiber was designed and constructed by coaxial electrospinning with the inner PLCL and outer gelatin. The morphology of the coaxial fiber was observed through TEM (Fig. 1A). The diameter distribution of the PLCL coaxial fiber without and with simvastatin loaded is shown in Figs 1B and 1C. The mean diameter of the PLCL/gelatin fibers is  $561 \pm 95$  nm, which increases to  $631 \pm 103$  nm in the drug-loaded group.

### 3.2. Characteristic of PLCL aerogel scaffold with simvastatin

Through a series of fabrication protocols, the PLCL/gelatin membranes and 3D aerogel scaffold were constructed and according to the simvastatin loaded or not, we set 4 groups. The microstructures in electron microscopy and the contact angle of 4 groups were displayed in Fig. 2. Comparing 4 groups, fibers in PLCL and PLCL@S were straight and crossing closely. But the fibers in the 2 aerogel groups showed more curled and loose with more space interlaced, especially in 3d-PLCL@S. Meanwhile, we can observe the fibers in simvastatin-loaded groups are thicker.

In addition, the hydrophilicity of the aerogel scaffold was analyzed by water contact angle measurements. The contact angle was decreasing from the left to the right in Fig. 2 (PLCL  $\theta = 123^\circ$ , PLCL@S  $\theta = 115^\circ$ , 3D-PLCL  $\theta = 52.2^\circ$ , 3D-PLCL@S  $\theta = 27.1^\circ$ ), demonstrating that aerogel scaffold with simvastatin bears better hydrophilicity than other groups. That means cells may grow more easily in this scaffold.

The simvastatin-releasing results of ultraviolet-visible spectrophotometry were shown in the amount chart (Fig. 1D). Drug concentration in 3D-PLCL@S solution increased to the peak at D4 and decreased gradient. However, the concentration of the PLCL@S group reached a peak on D2 and declined gradually. Generally, the concentration of 3D-PLCL@S was higher than PLCL@S every observation time, which means simvastatin could be releasing by degrees in the aerogel scaffold.

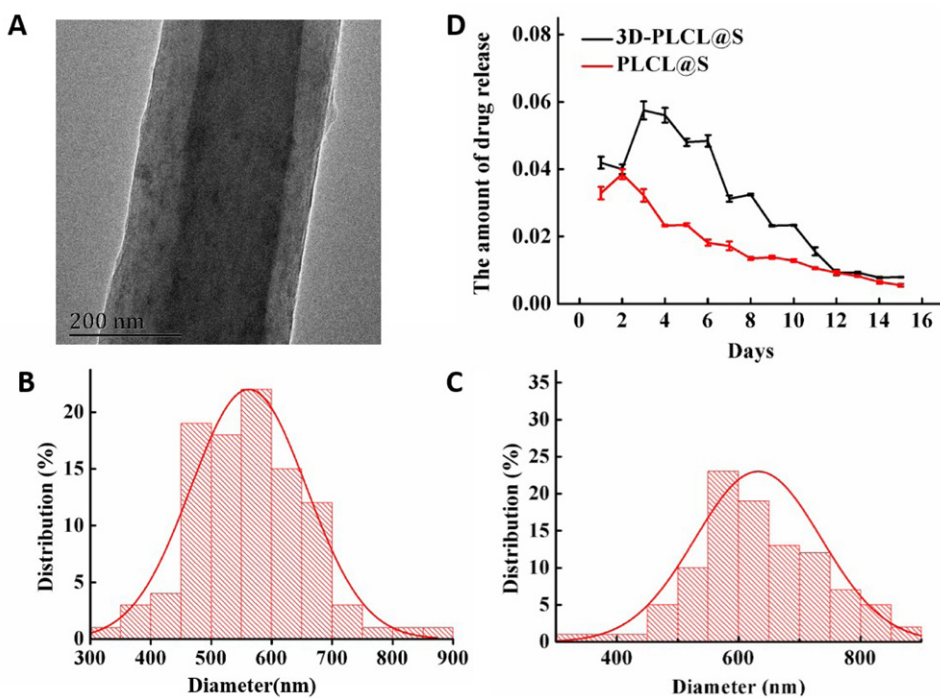


Fig. 1. Characteristic of PLCL aerogel scaffold with simvastatin. A: The morphology of the coaxial fiber with the inner PLCL and outer gelatin in TEM. B–C: The diameter distribution of the PLCL coaxial fiber without (B mean diameter  $561 \pm 95$  nm) and with simvastatin (C mean diameter  $631 \pm 103$  nm). D: The simvastatin-releasing curves of PLCL@S group (red curve) and 3D-PLCL@S group (black curve).

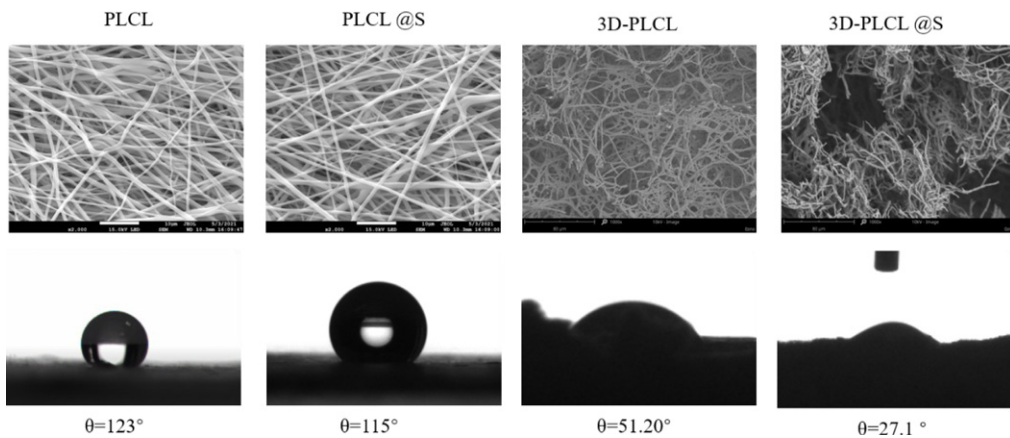


Fig. 2. The microstructures and contact angle of PLCL aerogel scaffold with simvastatin. The upper photos show the microstructure of 4 scaffolds (PLCL, 3D-PLCL, PLCL@S, 3D-PLCL@S) in SEM. The left two photos. The photos below display the contact angle ( $\theta$ ) of 4 scaffolds.

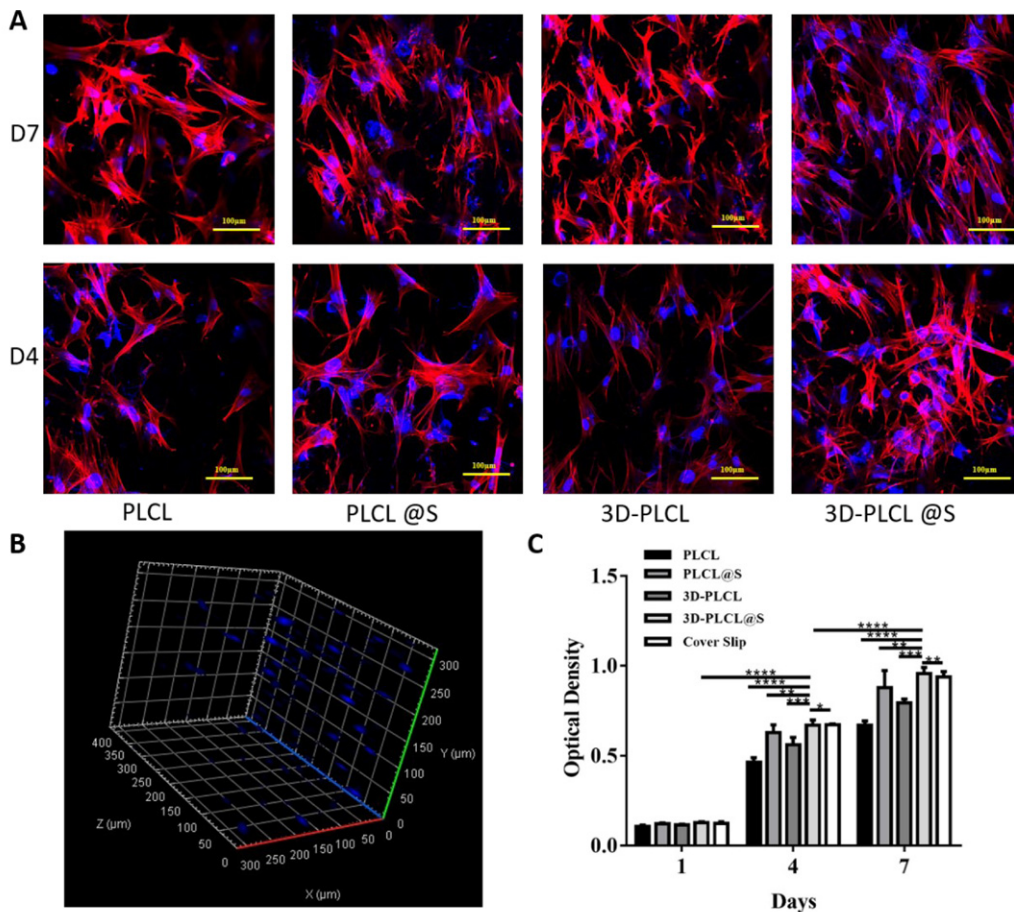


Fig. 3. Bioactivity of the drug-loaded aerogel scaffold. A. MC3T3-EI cells were cultured in the 4 different scaffolds and the cell morphology and proliferation at D4 and D7 were displayed with red F-actin and blue nucleus. B. Cells grow into the 3D-PLCL@S scaffold and 3D distribution was observed at D7 through ARIVIS VISION. C. Cell densities in 4 scaffolds and cover slip were calculated and exhibited in the chart. T test were conducted for the significance (\*means  $P < 0.05$ , \*\*means  $P < 0.01$ , \*\*\*means  $P < 0.001$ , \*\*\*\*means  $P < 0.0001$ ).

### 3.3. Bioactivity of the drug-loaded aerogel scaffold

We conducted an in vitro test with MC3T3-EI cells to confirm the biological response to the aerogel scaffold with simvastatin. Generally, cells exhibited similar morphology and chaotic arrangement on the different materials and the different time (Fig. 3A). Besides, cell density (cell counts per optical view) of 4 groups at D7 were higher than that at D4 respectively (Fig. 3C). We can also find that cell numbers in the 2 aerogel groups were visible higher than that in the other 2 groups. The cell numbers in groups with simvastatin count more than that without simvastatin, which declare that simvastatin may help cell proliferation to some extent. Through ARIVIS VISION, we got the 3D image of the 3D-PLCL@S group in D7 and we can observe cells growing into the aerogel material dispersedly (Fig. 3B). No significant difference was observed at D1. At D4 and D7, difference emerged and cell density in 3D-PLCL@S group

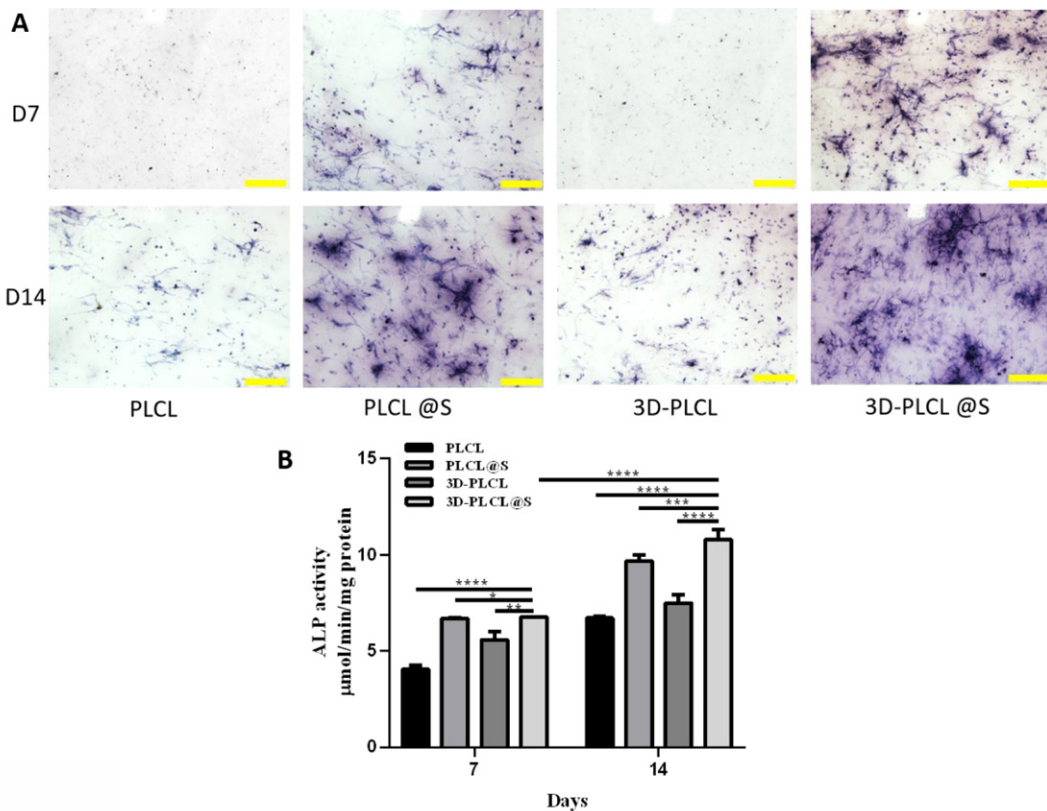


Fig. 4. Osteogenesis performance of 3D-PLCL@S scaffold in ALP staining. A. At D7 and D14, ALP staining experiment results were shown in 4 different groups (scale 200  $\mu$ m). B. ALP stain quantitative data was analyzed through imageJ. *T* test were conducted for the significance (\*means  $P < 0.05$ , \*\*means  $P < 0.01$ , \*\*\*means  $P < 0.001$ , \*\*\*\*means  $P < 0.0001$ ).

performed significantly better than other groups (D7: 3D-PLCL@S vs PLCL  $P < 0.0001$ , 3D-PLCL vs PLCL@S  $P < 0.01$ , 3D-PLCL vs 3D-PLCL@S  $P < 0.001$ , 3D-PLCL vs Cover Slip  $P < 0.01$ ).

### 3.4. Osteoblast differentiation

We conducted ALP staining and alizarin red S staining (ARS) to study osteoblast differentiation. The stain in groups with simvastatin was more massive than the groups without the drug and it bear the most remarkable stain at the D14 in the 3D-PLCL@S group (Fig. 4A). The ALP stain quantitative data were shown in Fig. 4B. From D7 to D14, ALP activity elevated significantly in 4 scaffolds, especially in 3D-PLCL@S (D7 vs D14  $P < 0.0001$ ). At D7 and D14, ALP activity in 3D-PLCL@S was significantly higher than that in other groups (D14: 3D-PLCL@S vs PLCL  $P < 0.0001$ , 3D-PLCL vs PLCL@S  $P < 0.001$ , 3D-PLCL vs 3D-PLCL@S  $P < .001$ ).

The ARS stain distribution and quantity in 3D-PLCL@S were better than others, corresponding to the ALP result (Fig. 5A). The ARS activity result was similar to ALP in Fig. 5B with the same analysis methods. From D7 to D14, ARS activity increased significantly in 4 scaffolds, especially in 3D-PLCL@S (D7 vs D14  $P < 0.0001$ ). At D7 and D14, ARS activity in 3D-PLCL@S was significantly higher

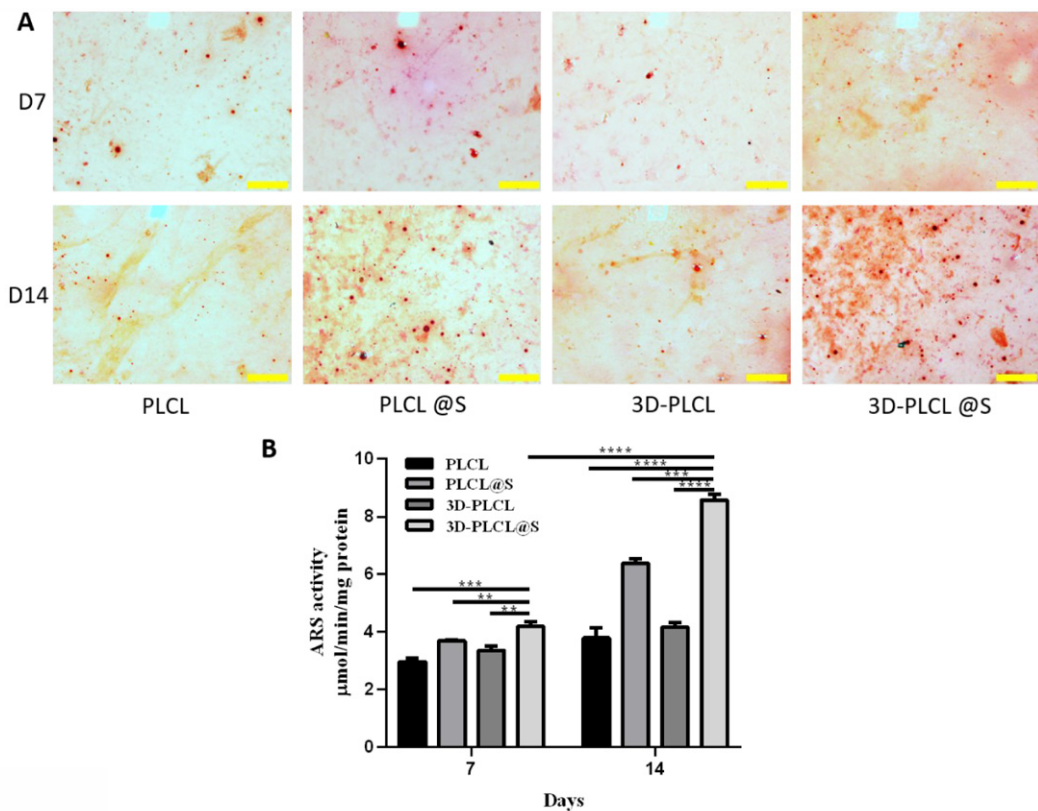


Fig. 5. Osteogenesis performance of 3D-PLCL@S scaffold in ARS staining. A. ARS staining photograph at D7 and D14 were shown in 4 different groups (scale 200  $\mu\text{m}$ ). B. ARS stain quantitative data was analyzed through imageJ. *T* test were conducted for the significance (\*\*means  $P < 0.01$ , \*\*\*means  $P < 0.001$ , \*\*\*\*means  $P < 0.0001$ ).

than that in other groups (D14: 3D-PLCL@S vs PLCL  $P < 0.0001$ , 3D-PLCL vs PLCL@S  $P < 0.001$ , 3D-PLCL vs 3D-PLCL@S  $P < 0.0001$ ).

#### 4. Discussion

Electrospinning is an important method used in traditional nanofiber scaffolds designed for tissue repair. Though it can mimic the extracellular matrix (ECM) of native tissue, its small nanofiber pore in two-dimensional (2D) structure restricts cell infiltration [22,23], which asks for the development of 3D scaffold to offer a better ECM analogue. We construct a novel 3D PLCL/gelatin coaxial fiber aerogel with the osteogenic factor simvastatin, in which osteoblast cells could grow into and promote bone regenerating [24–28]. Past research raised that aerogel would be a better scaffold for cell ossification [18] and thus we set a series of studies to verify the superiority of simvastatin loaded PLCL/gelatin aerogel scaffold in material science and biological compatibility.

We could observe the structure of 4 groups of material through the SEM, which shows fibers distributed more dispersive in two 3D aerogel groups. It could offer better contact angle results, that is, more hydrophilic and more suitable for the cell to plant on. Combined with the data of simvastatin improving

the diameter of the fiber and gradient releasing, 3D-PLCL@S demonstrates a more dispersive distribution of fibers and the minimum contact angle. The longer fiber diameter would be better for cell adherence. Thus, this contributes to biological comparability, which is an essential improvement for the scaffold of cell adherence and growth [29]. Meanwhile, simvastatin added shrank the contact angle and make it more beneficial and efficient for the cell to proliferate. The function of simvastatin promoting cell growth was reported in some research [30] and this is verified corresponding to our results.

Through observing 3D rendering, cells grow into the deep layer of the 3D-PLCL@S scaffold. The ARS and ADL experiments demonstrated that the cell could ossify more rapidly and effectively in the 3D-PLCL@S scaffold group. Despite live cell numbers resulting in more ossification in the 3D-PLCL@S scaffold group, the scaffold itself promoting the ossification of cells is unknown and remains to be verified further.

Statins, as an inhibitor of competitive 3-hydroxy-3-methyl coenzyme A (HMG-CoA) reductase, are widely used in hyperlipidemia treatment [31]. Simvastatin, as an inactive endolipid drug, functions in the liver through the conversion of the intracellular enzyme P450 to the ring-opening dihydroxyl type. It is reported that the drug promotes bone formation by inducing the expression of bone morphogenetic protein-2(BMP-2) [32,33]. Simvastatin could promote bone defect healing by combining two pathways of osteogenesis and angiogenesis [34,35]. However, it is difficult for simvastatin taking works hard on the human body because only a small dose of the drug could reach peripheral circulation. Some researches present that delivering simvastatin through local injection could solve the problem to reach the location with enough concentration but it leaves unstable concentration and local inflammation. This has been solved in our study that the scaffold could take control of releasing the simvastatin to maintain a high concentration locally in several days and accomplish the requirement of local release, avoiding the drawbacks of injection. Research *in vivo* in mice on whether the scaffold is a more suitable pro-osteogenic material is our next plan.

## 5. Conclusion

The PLCL/gelatin aerogel scaffold loaded with simvastatin make more sense in promoting osteoblast proliferation and osteogenic differentiation and we suppose that the scaffold could be a potential material for the bone defect.

## Author contributions

Lai Linfeng: Methodology, Formal analysis, Writing-Original Draft, and Visualization. Zhou Xiaowei: Methodology and Formal analysis. Chen Xueqin: Resources, Validation. Zhu Xianfeng: Conceptualization, Project administration and Writing-Review & Editing.

## Conflict of interest

The authors declare that they have no conflict of interest.

## Funding

This work is supported by the Wenzhou Science and Technology Bureau program “Simvastatin-loaded 3D aerogel scaffolds promote bone regeneration” (No. 2022Y1050, Lai Linfeng).

## References

- [1] L. Li, F. Yu, J. Shi, S. Shen, H. Teng, J. Yang et al., In situ repair of bone and cartilage defects using 3D scanning and 3D printing, *Sci Rep* **7**(1) (2017), 9416.
- [2] C. Lin, Y. Wang, Z. Huang, T. Wu, W. Xu, W. Wu et al., Advances in filament structure of 3D bioprinted biodegradable bone repair scaffolds, *Int J Bioprint* **7**(4) (2021), 426.
- [3] R.T. Annamalai, X. Hong, N.G. Schott, G. Tiruchinapally, B. Levi and J.P. Stegemann, Injectable osteogenic microtissues containing mesenchymal stromal cells conformally fill and repair critical-size defects, *Biomaterials* **208** (2019), 32–44.
- [4] E.H. Schemitsch, Size matters: Defining critical in bone defect size! *J Orthop Trauma* **31**(Suppl 5) (2017), S20–S22.
- [5] X. Zhang, Y. Li, Y.E. Chen, J. Chen and P.X. Ma, Cell-free 3D scaffold with two-stage delivery of miRNA-26a to regenerate critical-sized bone defects, *Nat Commun* **7** (2016), 10376.
- [6] S. Almubarak, H. Nethercott, M. Freeberg, C. Beaudon, A. Jha, W. Jackson et al., Tissue engineering strategies for promoting vascularized bone regeneration, *Bone* **83** (2016), 197–209.
- [7] J.A. Kim, J. Lim, R. Naren, H.S. Yun and E.K. Park, Effect of the biodegradation rate controlled by pore structures in magnesium phosphate ceramic scaffolds on bone tissue regeneration in vivo, *Acta Biomater* **44** (2016), 155–167.
- [8] J. Rouwkema, N.C. Rivron and C.A. van Blitterswijk, Vascularization in tissue engineering, *Trends Biotechnol* **26**(8) (2008), 434–441.
- [9] D.F. Williams, On the mechanisms of biocompatibility, *Biomaterials* **29**(20) (2008), 2941–2953.
- [10] Y. Yao, W. Qin, B. Xing, N. Sha, T. Jiao and Z. Zhao, High performance hydroxyapatite ceramics and a triply periodic minimum surface structure fabricated by digital light processing 3D printing, *J Adv Ceram* **10**(1) (2021), 39–48.
- [11] M.J. Olszta, X. Cheng, S.S. Jee, R. Kumar, Y. Kim, M.J. Kaufman et al., Bone structure and formation: A new perspective, *Materials Science and Engineering: R: Reports* **58**(3–5) (2007), 77–116.
- [12] A.L. Boskey, Erratum: Bone composition: relationship to bone fragility and antiosteoporotic drug effects, *Bonekey Rep* **4** (2015), 710.
- [13] S. Fu, M. Zhu and Y. Zhu, Organosilicon polymer-derived ceramics: An overview, *J Adv Ceram* **8**(4) (2019), 457–478.
- [14] G.L. Ying, N. Jiang, S. Maharjan, Y.X. Yin, R.R. Chai, X. Cao et al., Aqueous two-phase emulsion bioink-enabled 3D bioprinting of porous hydrogels, *Adv Mater* **30**(50) (2018), e1805460.
- [15] X. Wang, M. Jiang, Z. Zhou, J. Gou and D. Hui, 3D printing of polymer matrix composites: A review and prospective, *Composites Part B: Engineering* **110** (2017), 442–458.
- [16] S. Araby, A. Qiu, R. Wang, Z. Zhao, C. Wang and J. Ma, Aerogels based on carbon nanomaterials, *J Mater Sci* **51**(20) (2016), 9157–9189.
- [17] A.C. Pierre and G.M. Pajonk, Chemistry of aerogels and their applications, *Chem Rev* **102**(11) (2002), 4243–4265.
- [18] L. Weng, S.K. Boda, H. Wang, M.J. Teusink, F.D. Shuler and J. Xie, Novel 3D hybrid nanofiber aerogels coupled with BMP-2 peptides for cranial bone regeneration, *Adv Healthc Mater* **7**(10) (2018), e1701415.
- [19] Y. Xue, M. Wu, Z. Liu, J. Song, S. Luo, H. Li et al., In vitro and in vivo evaluation of chitosan scaffolds combined with simvastatin-loaded nanoparticles for guided bone regeneration, *J Mater Sci Mater Med* **30**(4) (2019), 47.
- [20] E. Barrios, D. Fox, S.Y. Li, R. Catarata, J.E. Calderon, N. Azim et al., Nanomaterials in advanced, high-performance aerogel composites: A review, *Polymers (Basel)* **11**(4) (2019), 726.
- [21] Y. Cho, J. Hong, H. Ryoo, D. Kim, J. Park and J. Han, Osteogenic responses to zirconia with hydroxyapatite coating by aerosol deposition, *J Dent Res* **94**(3) (2015), 491–499.
- [22] T. Lu, Y. Li and T. Chen, Techniques for fabrication and construction of three-dimensional scaffolds for tissue engineering, *Int J Nanomedicine* **8** (2013), 337–350.
- [23] R.L. Dahlin, F.K. Kasper and A.G. Mikos, Polymeric nanofibers in tissue engineering, *Tissue Eng Part B Rev* **17**(5) (2011), 349–364.
- [24] V. Thomas, X. Zhang, S.A. Catledge and Y.K. Vohra, Functionally graded electrospun scaffolds with tunable mechanical properties for vascular tissue regeneration, *Biomed Mater* **2**(4) (2007), 224–232.
- [25] C. Erisken, D.M. Kalyon and H. Wang, Functionally graded electrospun polycaprolactone and  $\beta$ -tricalcium phosphate nanocomposites for tissue engineering applications, *Biomaterials* **29**(30) (2008), 4065–4073.

- [26] V. Thomas, X. Zhang and Y.K. Vohra, A biomimetic tubular scaffold with spatially designed nanofibers of protein/PDS bio-blends, *Biotechnol Bioeng* **104**(5) (2009), 1025–1033.
- [27] X. Zhang, V. Thomas and Y.K. Vohra, In vitro biodegradation of designed tubular scaffolds of electrospun protein/polyglyconate blend fibers, *J Biomed Mater Res B Appl Biomater* **89**(1) (2009), 135–147.
- [28] M.J. McClure, S.A. Sell, D.G. Simpson, B.H. Walpoth and G.L. Bowlin, A three-layered electrospun matrix to mimic native arterial architecture using polycaprolactone, elastin, and collagen: A preliminary study, *Acta Biomater* **6**(7) (2010), 2422–2433.
- [29] F. Rupp, L. Scheideler, N. Olshanska, M. de Wild, M. Wieland and J. Geis-Gerstorfer, Enhancing surface free energy and hydrophilicity through chemical modification of microstructured titanium implant surfaces, *J Biomed Mater Res A* **76**(2) (2006), 323–334.
- [30] W.L. Yu, T.W. Sun, C. Qi, H.K. Zhao, Z.Y. Ding, Z.W. Zhang et al., Enhanced osteogenesis and angiogenesis by mesoporous hydroxyapatite microspheres-derived simvastatin sustained release system for superior bone regeneration, *Sci Rep* **7** (2017), 44129.
- [31] M. Sonobe, K. Hattori, N. Tomita, T. Yoshikawa, H. Aoki, Y. Takakura et al., Stimulatory effects of statins on bone marrow-derived mesenchymal stem cells. Study of a new therapeutic agent for fracture, *Biomed Mater Eng* **15**(4) (2005), 261–267.
- [32] M. Weis, C. Heeschen, A.J. Glassford and J.P. Cooke, Statins have biphasic effects on angiogenesis, *Circulation* **105**(6) (2002), 739–745.
- [33] K.Y. Choi, H.J. Kim, M.H. Lee, T.G. Kwon, H.D. Nah, T. Furuichi et al., Runx2 regulates FGF2-induced Bmp2 expression during cranial bone development, *Dev Dyn* **233**(1) (2005), 115–121.
- [34] P.J. Bouletreau, S.M. Warren, J.A. Spector, Z.M. Peled, R.P. Gerrets, J.A. Greenwald et al., Hypoxia and VEGF up-regulate BMP-2 mRNA and protein expression in microvascular endothelial cells: Implications for fracture healing, *Plast Reconstr Surg* **109**(7) (2002), 2384–2397.
- [35] K.H. Baek, W.Y. Lee, K.W. Oh, H.J. Tae, J.M. Lee, E.J. Lee et al., Lee dayhuman bone marrow stromal cells, *J Korean Med Sci* **20**(3) (2005), 438–444.